Quantitative characterization of the path of glucose diffusion facilitated by human glucose transporter 1

Liao Y. Chen[1]*

From the [1]Department of Physics and Astronomy, The University of Texas at San Antonio, San Antonio, Texas 78249

Running title: *GLUT1 conducts glucose through a fluctuating gate*

* To whom correspondence should be addressed: Liao Y. Chen: Department of Physics & Astronomy, The University of Texas at San Antonio, One UTSA Circle, San Antonio, Texas 78249; Liao.Chen@utsa.edu; Tel. (210) 458-5457; Fax. (210)458-4919.

Keywords: glucose transport, membrane transport, protein-lipid interaction, membrane lipid, thermodynamics, molecular dynamics

ABSTRACT

Glucose transporter GLUT1 is ubiquitously expressed in the human body from the red cells to the blood-brain barrier to the skeletal muscles. It is physiologically relevant to understand how GLUT1 facilitates diffusion of glucose across the cell membrane. It is also pathologically relevant because GLUT1 deficiency causes neurological disorders and anemia and because GLUT1 overexpression fuels the abnormal growth of cancer cells. This article presents a quantitative investigation of GLUT1 based on all-atom molecular-dynamics (MD) simulations of the transporter embedded in lipid bilayers of asymmetric inner-and-outer-leaflet lipid compositions, subject to asymmetric intra-and-extra-cellular environments. This is in contrast with the current literature of MD studies of the transporter embedded in a symmetric lipid bilayer of a single lipid type. The equilibrium (unbiased) dynamics of GLUT1 shows that it can facilitate glucose diffusion across the cell membrane without undergoing large-scale conformational motions. The Gibbs free-energy profile, which is still lacking in the current literature of GLUT1, quantitatively characterizes the diffusion path of glucose from the periplasm, through an extracellular gate of GLUT1, on to the binding site, and off to the cytoplasm. This transport mechanism is validated by the experimental data that GLUT1 has low water-permeability, high glucose-affinity, uptake-efflux symmetry, and 10 kcal/mol Arrhenius activation barrier around 37°C.

INTRODUCTION

Thirteen isoforms of glucose transporters (GLUTs)(1-4) are expressed throughout the human body to facilitate a major form of energy metabolism(5-17). Deficiency in or mutations of GLUTs were found to cause severe health problems(5,18-25). In particular, GLUT1(26-29), encoded by *SLC2A1,* is richly expressed in endothelial cells of the blood–brain barrier(7,17,30-32). Deficiency in GLUT1 causes neurological disorders, for example. GLUT1 is replete in erythrocytes(27,29,33) and, in fact, it outnumbers water channel protein AQP1(34) that is also very richly expressed in human erythrocytes(33) for hydrohomeostasis. Naturally, GLUT1 has been a subject of many investigations due to its physiological and pathological relevance and due to its abundant availability from erythrocytes.

The structure of GLUT1, like other transporters in the major facilitator superfamily (MFS), has been shown to have a conserved core fold of 12 transmembrane (TM) segments organized into two discrete domains, the

amino- and carboxy-terminal (N- and C-) domains(29,35-40). And, recently, the crystal structures of GLUT1 have been resolved to atomistic accuracy(39,40). In the rich literature of kinetics experiments on GLUT1 (reviewed in, *e.g.*, (41,42)), it is unambiguous that glucose transport is symmetric between uptake and efflux both of which are very rapid at near-physiological temperatures. The Arrhenius activation barrier of glucose transport is approximately 10 kcal/mol(42). It is also unambiguous that GLUT1, even though outnumbering AQP1, does not contribute significantly to water transport across the erythrocyte membrane(43).

On the theoretical-computational side, there are many more questions than answers about this ubiquitous transporter. Most molecular dynamics (MD) simulations, *e.g.*, (44-47), were focused on conforming with the alternating access theory(1,48) that is thought to be universally applicable for all MFS transporters including GLUT1. All these and most other MD simulations on GLUTs (44-47,49-51) have the cell membrane modelled as a symmetric bilayer of a single lipid type. They do not heed the known facts that the structure and activities of GLUTs are sensitive to the membrane lipid compositions.(52-56) In particular, glucose transport across erythrocyte membranes was found, long ago, to be reduced by 75% by exposure to phospholipase A2 which hydrolyzes fatty acyl groups from the sn-2 position of glycerophospholipids.(54,56) In general, lipid-protein interactions are significant determinants of the membrane protein functions.(57-60) It is natural and fundamental to ask: What are the dynamic characteristics of GLUT1 embedded in a membrane of inner-and-outer-leaflet asymmetric lipid compositions? Furthermore, in all GLUT1 simulations of the current literature, the intracellular (IC) and the extracellular (EC) sides are artifactitiously mixed as technically required by the computing technique of electrostatic interactions. Consequently, the asymmetry between the IC saline and the EC saline is lost in these simulations and thus is the membrane potential. How does the loss of IC-EC asymmetry in simulations alter the GLUT1 dynamics? More importantly, how does GLUT1 facilitate glucose diffusion across the cell membrane? Can we elucidate (without *a priori* assumptions) the transport mechanism from a model system with necessary regard to the lipid compositions and IC-EC asymmetry of a biological cell? Can we quantitatively characterize the path of glucose diffusion through GLUT1 in terms of the Gibbs free energy in agreement with the experimental data?

This article answers the aforementioned questions through MD simulations of an all-atom model of GLUT1 in IC-EC asymmetric environments mimicking the human erythrocyte(61,62) (illustrated in Fig. 1 and in the supporting information (SI), Fig. S1). In this model system, the asymmetry is considered in lipid compositions of the inner and the outer leaflets of the cell membrane. Also considered is the asymmetry in the IC saline consisting mostly of KCl and the EC saline consisting mostly of NaCl. The equilibrium unbiased MD and the steered MD (SMD) simulations were implemented with double-precision computations throughout. From the full electrostatics, the membrane potential was computed at ~75 mV. From the long-time dynamics (unbiased equilibrium MD) of GLUT1 in asymmetric IC-EC environments, GLUT1 is shown to facilitate glucose diffusion across the cell membrane along a transport path through a fluctuating EC gate, *via* the binding site, and through wide opening on the IC side while remaining in the endofacial conformation. The transport path is lined up with residues that favor glucose affinity and disfavors water permeation. From the SMD simulations, the Gibbs free-energy profile of glucose transport was computed in quantitative agreement with the experimental data.

RESULTS AND DISCUSSION

Fig. 1 and SI, Fig. S1 show the model system for which 500 ns equilibrium (unbiased) MD run was conducted at the physiological temperature 37°C. In order to accurately compute the long-range electrostatic interactions with the particle mesh Ewald (PME) technique, periodic boundary conditions (PBC) are applied

in all three dimensions. The use of PBC leads to artifactitious mixing between the left-hand side with the right-hand side of the model system (Fig. 1, bottom panel). In this study, the model system, the unit cell under the PBC, consists of two patches of GLUT1-embedded membranes (Fig. 1 and SI, Fig. S1) that separate the IC space in between the two patches from the EC space outside the two membranes. The artifactitious mixing is only between the EC sides of the adjacent unit cells. The IC saline and the EC saline are not artifactitiously mixed by the PBC. Any exchange of water or solutes between the IC and the EC can only happen *via* transport across the cell membrane. Consequently, the IC-EC asymmetry is not lost in the PME-based simulations of this work. The IC saline contains 150 mM KCl while the EC saline has 150 mM NaCl. Furthermore, the inner leaflet of the membrane consists of 20% cholesterol, 11% POPC, 38% POPE, 22% POPS, and 9% SSM while the outer leaflet has 20% cholesterol, 35% POPC, 10% POPE, and 35% SSM)(61,62). The two GLUT1 proteins, one on each membrane patch, are oriented in the native orientation in erythrocytes.

To illustrate that this model "cell" system is a valid approximation to the human erythrocyte, the charge distribution of the system was computed from the last 100 ns of the 500 ns MD run. The Poisson equation for the electrostatic potential was integrated along the z-axis for the membrane potential shown in Fig. 1. The mean value and the standard error were taken from the statistics over the last 100 ns of the 500 ns MD simulation. The potential difference between the IC surface of the membrane and the EC surface of the membrane is approximately -70 mV which is a reasonable approximation for the human erythrocyte. This validates the choice of lipids for the inner and the outer leaflets. Interestingly, there is a potential difference of ~35 mV from the IC membrane surface to the IC bulk region. This 35mV potential difference should be dependent upon the ion compositions in the IC fluid. Improvement of the approximation can be furthered with fine tuning the ion compositions of the model system, which is unnecessary in this present study of transport of neutral solutes but will be necessary for any studies of ion transport.

Figs. 2 and 3 show the long-time dynamics of GLUT1 subject to asymmetric IC-EC environments. For both proteins embedded in the two membrane patches, the dynamics is represented by small fluctuations around the crystal structure. During 500 ns of equilibrium dynamics at 37°C, the protein conformational changes are small and both proteins remain in the endofacial conformation observed in the crystal structure(39,40) (Fig. 2). The deviations from the crystal structure are mainly from the relatively large sidechain fluctuations and the small shifting of the transmembrane helices. In fact, the deviation as a function of time stabilizes after the initial 100 ns and remains fluctuating around 2.2 Å (Fig. 3(B)). Interestingly, once the protein dynamics stabilizes at ~100 ns, a gate on the EC side opens and fluctuates between the open and the closed state. When the EC gate is open, the glucose binding site inside the protein is accessible from the EC side while it is invariably open to the IC. The EC gate, shown in Fig. 3, consists of four groups of residues on four transmembrane helices: (1) Gly31, Val32, Ile33, Asn34, Ala35, and Pro36 (green colored) are located from the EC end of TM1 to the beginning of EC helix 1. (2) Val165, Val166, Gly167, Ile168, Leu169, Ile170, Ala171, Gln172, Val173, and Phe174 (orange colored) on the EC end of TM5. (3) Val290, Phe291, Tyr292, Tyr293, Ser294, Thr295, Ser296, Ile297, Phe298, and Glu299 (tan colored) on the EC end of TM7 and the EC helix connection to TM8. (4) Gln305, Pro306, Val307, Tyr308, Ala309, Thr310, Ile311, Gly312, Ser313, Gly314, Ile315, Val316, and Asn317 (purple colored) on the EC end of TM8. Qualitatively, the GLUT1 dynamics are similar to the case studied in Ref. (53) where GLUT1 was embedded in a single membrane patch that had similar lipid compositions. Quantitatively, the EC gate is open for ~10% of the time which is much shorter than in the single-membrane model where the gate is nearly open all the time at 37°C. Some additional details are available in SI.

Fig. 4 illustrates the path of glucose transport through GLUT1. It is known that

GLUT1 is a passive facilitator for glucose diffusion down the concentration gradient. The driving force for glucose transport is the Gibbs free-energy gradient along the diffusion path. Experimental data of kinetics showed an Arrhenius activation barrier ~10 kcal/mol around 37°C.(42) This high barrier renders it infeasible to compute the free-energy profile directly from equilibrium MD simulations. Shown in the top panel of Fig. 4 are the results of 744 ns SMD runs.

Starting from the binding site ($z = 0$ Å), the glucose molecule was pulled/steered forward and backward over sections of 1 Å each: 32 sections to the IC side and 28 sections to the EC side. In each section, the center-of-mass z-coordinate of glucose was steered at a speed of 1 Å/ns along the z-axis in the sampling of a forward path and along the negative z-direction in the sampling of a reverse path. The pulling was repeated 4 times to sample 4 forward and 4 reverse paths in each section. At the end of every section, the system was equilibrated for 4 ns while the z-coordinate of glucose's center of mass was fixed. The x- and y-coordinates of the glucose center of mass were free to follow the stochastic dynamics of the system. The work done to the system along the forward paths and that along the reverse paths both contain irreversible dissipative work in addition to the reversible change in the Gibbs free energy. The use of the Brownian dynamics fluctuation-dissipation theorem had those two parts cancelled to yield the reversible potential of mean force (PMF) as a function of z shown in Fig. 4, namely, the Gibbs free energy of the system when the center-of-mass z-coordinate of the glucose is fixed at a given value.(63)

Going along the glucose diffusion path from the EC side ($z\sim -30$ Å), through the EC gate, down to the binding site ($z\sim 0$ Å) and from there up to the IC side ($z\sim 30$ Å), the free-energy difference between the IC and the EC is approximately zero. The equal levels on the two sides are required for passive diffusion of neutral solutes down the concentration gradient. Discrepancy from this equality indicates the inaccuracy of a computational work. On the EC side, through the EC gate, the PMF curve exhibits minor dips and bumps, which reflects that the EC gate constantly fluctuates between closed and open states. The EC-gating residues are flexible to allow glucose passage without significant water flux through there. The PMF at the binding site is approximately 10 kcal/mol below the EC or IC level. This agrees with the experimental fact of glucose-GLUT1 affinity. Each glucose transport event, either uptake or efflux, consists of two parts: falling into the binding site with a PMF drop of 10 kcal/mol and climbing out of there with a PMF rise of 10 kcal/mol. This thermal activation nature of glucose transport quantitatively agrees with the experimental data of 10 kcal/mol in Arrhenius activation barrier around 37°C. (42)

The residues along the glucose transport path: Phe26, Thr30, Gly31, Asn34, Ala35, Gln37, Lys38, Thr137, Pro141, Arg153, Gly154, Gly157, His160, Gln161, Ile164, Ile168, Gln172, Leu176, Gln282, Gln283, Ile287, Asn288, Phe291, Tyr292, Ser294, Thr295, Val307, Thr310, Glu329, Arg333, Trp388, Phe389, Gly408, Asn411, and Asn415 (illustrated in Fig. 4). It is interesting to note that 30 of these 35 residues are conserved between human GLUT1 and GLUT3. (53) The many aromatic residues along the path provide affinity for glucose and hydrophobicity to disfavor water passage. All these, in agreement with experimental findings, indicate validity of this research.

METHODS

We took the high-resolution crystal structure of GLUT1 (PDB code: 4PYP)(39), mutated it back to wild type, replaced β-nonylglucoside with β-D-glucose, translated and rotated the sugar-protein complex so that its center is located at the origin of the Cartesian coordinates and its orientation is such that the z-axis points to the IC side, embedded the complex in a patch of lipid bilayer consisting of multiple types of lipids (the IC leaflet consists of 20% cholesterol, 11% POPC, 38% POPE, 22% POPS, and 9% SSM while the EC leaflet has 20% cholesterol, 35% POPC, 10% POPE, and 35% SSM),(61,62) solvated the sugar-protein-membrane complex with a cubic box of water, and then added sodium/potassium and chloride ions to neutralize the net charges of the system and to salinate the system with

150 mM KCl on the IC side and 150 mM NaCl on the EC side. We replicated this single-patch system, inverted the replicate, placed it right next to the original to form the two-patch system shown in SI, Fig. S1. The total system consists of 290,726 atoms. Its dimensions are $108\text{Å} \times 108\text{Å} \times 246\text{Å}$ when fully equilibrated.

CHARMM36 force field parameters(64,65) and NAMD(66) were employed for all simulations at the constant temperature of 37°C and the constant pressure of 1 bar using the Langevin pistons. The CHARMM GUI(67,68) was used to embed the GLUT1-sugar complex into the lipid bilayer. The PME was implemented on $128 \times 128 \times 256$ grids for full electrostatic interactions. All the procedures and parameters not specified here are identical to (50).

For GLUT1 dynamics, we conducted 500 ns production run of MD without any biases/constraints beyond the initial procedures of building and equilibrating the system components. For the free-energy profile of glucose diffusion through GLUT1, we followed the multi-sectional approach of (63) to conduct 60 sets of SMD runs to cover the entire diffusion path from the EC to the IC side for a total z-displacement of 60 Å. Over each 1 Å section, the center-of-mass z-coordinate of glucose was pulled/steered at a velocity of 1 Å/ns to sample a forward path and at a velocity of -1 Å/ns to sample a reverse path. At the end of each section, the system was equilibrated for 4 ns while fixing the center-of-mass z-coordinate of glucose. With a total 744 ns SMD simulations, we sampled 4 forward and 4 reverse paths and computed the PMF along the glucose diffusion path, *i.e.,* the Gibbs free energy of the system when the center-of-mass z-coordinate of glucose is fixed at a given value. The standard errors were over the 4 sets of forward and reverse paths.

Supporting Information: Three videos and five additional figures that are discussed but not included in the main text.

Data availability: The Dataset (parameters, coordinates, scripts, *etc.*) to replicate this study is available at Harvard Dataverse, https://doi.org/10.7910/DVN/KTRQJ4.

Acknowledgements: The author acknowledges the computing resources provided by the Texas Advanced Computing Center (TACC) at the University of Texas at Austin.

Conflict of interest: The author declares that he has no conflicts of interest with the contents of this article.

REFERENCES

1. Nelson, D. L., and Cox, M. M. (2005) *Lehninger Principles of Biochemistry*, 4th ed., W. H. Freeman and Co, New York
2. Carruthers, A. (1990) Facilitated diffusion of glucose. *Physiological Reviews* **70**, 1135-1176
3. Mueckler, M., and Thorens, B. (2013) The SLC2 (GLUT) family of membrane transporters. *Molecular Aspects of Medicine* **34**, 121-138
4. Yan, N. (2017) A Glimpse of Membrane Transport through Structures—Advances in the Structural Biology of the GLUT Glucose Transporters. *Journal of Molecular Biology* **429**, 2710-2725
5. Augustin, R. (2010) The protein family of glucose transport facilitators: It's not only about glucose after all. *IUBMB Life* **62**, 315-333
6. Thorens, B., and Mueckler, M. (2010) Glucose transporters in the 21st Century. *American Journal of Physiology - Endocrinology And Metabolism* **298**, E141

7. Harik, S. I., Hall, A. K., Richey, P., Andersson, L., Lundahl, P., and Perry, G. (1993) Ontogeny of the erythroid/HepG2-type glucose transporter (GLUT-1) in the rat nervous system. *Developmental brain research* **72**, 41-49
8. Simpson, I. A., Dwyer, D., Malide, D., Moley, K. H., Travis, A., and Vannucci, S. J. (2008) The facilitative glucose transporter GLUT3: 20 years of distinction. *American Journal of Physiology - Endocrinology And Metabolism* **295**, E242
9. Cushman, S. W., and Wardzala, L. J. (1980) Potential mechanism of insulin action on glucose transport in the isolated rat adipose cell. Apparent translocation of intracellular transport systems to the plasma membrane. *Journal of Biological Chemistry* **255**, 4758-4762
10. Suzuki, K., and Kono, T. (1980) Evidence that insulin causes translocation of glucose transport activity to the plasma membrane from an intracellular storage site. *Proceedings of the National Academy of Sciences of the United States of America* **77**, 2542-2545
11. Thorens, B. (1992) Molecular and Cellular Physiology of GLUT-2, a High-KmFacilitated Diffusion Glucose Transporter. in *International Review of Cytology* (Friedlander, M., and Mueckler, M. eds.), Academic Press. pp 209-238
12. Uldry, M., and Thorens, B. (2004) The SLC2 family of facilitated hexose and polyol transporters. *Pflügers Archiv* **447**, 480-489
13. Kalaria, R. N., Gravina, S. A., Schmidley, J. W., Perry, G., and Harik, S. I. (1988) The glucose transporter of the human brain and blood-brain barrier. *Annals of Neurology* **24**, 757-764
14. Maher, F., and Simpson, I. A. (1994) The GLUT3 glucose transporter is the predominant isoform in primary cultured neurons: assessment by biosynthetic and photoaffinity labelling. *Biochemical Journal* **301**, 379-384
15. Furler, S. M., Jenkins, A. B., Storlien, L. H., and Kraegen, E. W. (1991) In vivo location of the rate-limiting step of hexose uptake in muscle and brain tissue of rats. *American Journal of Physiology - Endocrinology And Metabolism* **261**, E337
16. Ziel, F. H., Venkatesan, N., and Davidson, M. B. (1988) Glucose Transport Is Rate Limiting for Skeletal Muscle Glucose Metabolism in Normal and STZ-Induced Diabetic Rats. *Diabetes* **37**, 885
17. Simpson, I. A., Vannucci, S. J., and Maher, F. (1994) Glucose transporters in mammalian brain. *Biochemical Society Transactions* **22**, 671
18. Bannasch, D., Safra, N., Young, A., Karmi, N., Schaible, R. S., and Ling, G. V. (2008) Mutations in the SLC2A9 Gene Cause Hyperuricosuria and Hyperuricemia in the Dog. *PLOS Genetics* **4**, e1000246
19. Yang, H., Wang, D., Engelstad, K., Bagay, L., Wei, Y., Rotstein, M., Aggarwal, V., Levy, B., Ma, L., Chung Wendy, K., and De Vivo Darryl, C. (2011) Glut1 deficiency syndrome and erythrocyte glucose uptake assay. *Annals of Neurology* **70**, 996-1005
20. De Vivo, D. C., Wang, D., Pascual, J. M., and Ho, Y. Y. (2002) Glucose transporter protein syndromes. in *International Review of Neurobiology* (Dwyer, D. S. ed.), Academic Press. pp 259-288
21. An, Y., Varma, V. R., Varma, S., Casanova, R., Dammer, E., Pletnikova, O., Chia, C. W., Egan, J. M., Ferrucci, L., Troncoso, J., Levey, A. I., Lah, J., Seyfried, N. T., Legido-Quigley, C., O'Brien, R., and Thambisetty, M. (2018) Evidence for brain glucose dysregulation in Alzheimer's disease. *Alzheimer's & Dementia: The Journal of the Alzheimer's Association* **14**, 318-329
22. Adekola, K., Rosen, S. T., and Shanmugam, M. (2012) Glucose transporters in cancer metabolism. *Current Opinion in Oncology* **24**, 650-654
23. McCracken, A. N., and Edinger, A. L. (2013) Nutrient transporters: the Achilles heel of anabolism. *Trends in Endocrinology & Metabolism* **24**, 200-208

24. Younes, M., Brown, R. W., Stephenson, M., Gondo, M., and Cagle, P. T. (1997) Overexpression of Glut1 and Glut3 in stage I nonsmall cell lung carcinoma is associated with poor survival. *Cancer* **80**, 1046-1051
25. Yamamoto, T., Seino, Y., Fukumoto, H., Koh, G., Yano, H., Inagaki, N., Yamada, Y., Inoue, K., Manabe, T., and Imura, H. (1990) Over-expression of facilitative glucose transporter genes in human cancer. *Biochemical and Biophysical Research Communications* **170**, 223-230
26. Baldwin, S. A., and Lienhard, G. E. (1989) Purification and reconstitution of glucose transporter from human erythrocytes. in *Methods in Enzymology*, Academic Press. pp 39-50
27. Kasahara, M., and Hinkle, P. C. (1977) Reconstitution and purification of the D-glucose transporter from human erythrocytes. *Journal of Biological Chemistry* **252**, 7384-7390
28. Birnbaum, M. J., Haspel, H. C., and Rosen, O. M. (1986) Cloning and characterization of a cDNA encoding the rat brain glucose-transporter protein. *Proceedings of the National Academy of Sciences* **83**, 5784
29. Mueckler, M., Caruso, C., Baldwin, S. A., Panico, M., Blench, I., Morris, H. R., Allard, W. J., Lienhard, G. E., and Lodish, H. F. (1985) Sequence and structure of a human glucose transporter. *Science* **229**, 941
30. Dick, A. P., Harik, S. I., Klip, A., and Walker, D. M. (1984) Identification and characterization of the glucose transporter of the blood-brain barrier by cytochalasin B binding and immunological reactivity. *Proceedings of the National Academy of Sciences* **81**, 7233
31. Maher, F., Vannucci, S. J., and Simpson, I. A. (1994) Glucose transporter proteins in brain. *The FASEB Journal* **8**, 1003-1011
32. Pardridge, W. M., Boado, R. J., and Farrell, C. R. (1990) Brain-type glucose transporter (GLUT-1) is selectively localized to the blood-brain barrier. Studies with quantitative western blotting and in situ hybridization. *Journal of Biological Chemistry* **265**, 18035-18040
33. Bryk, A. H., and Wiśniewski, J. R. (2017) Quantitative Analysis of Human Red Blood Cell Proteome. *Journal of Proteome Research* **16**, 2752-2761
34. Zeidel, M. L., Ambudkar, S. V., Smith, B. L., and Agre, P. (1992) Reconstitution of functional water channels in liposomes containing purified red cell CHIP28 protein. *Biochemistry* **31**, 7436-7440
35. Hresko, R. C., Kruse, M., Strube, M., and Mueckler, M. (1994) Topology of the Glut 1 glucose transporter deduced from glycosylation scanning mutagenesis. *Journal of Biological Chemistry* **269**, 20482-20488
36. Blodgett, D. M., Graybill, C., and Carruthers, A. (2008) Analysis of Glucose Transporter Topology and Structural Dynamics. *Journal of Biological Chemistry* **283**, 36416-36424
37. Radestock, S., and Forrest, L. R. (2011) The Alternating-Access Mechanism of MFS Transporters Arises from Inverted-Topology Repeats. *Journal of Molecular Biology* **407**, 698-715
38. Shi, Y. (2013) Common Folds and Transport Mechanisms of Secondary Active Transporters. *Annual Review of Biophysics* **42**, 51-72
39. Deng, D., Xu, C., Sun, P., Wu, J., Yan, C., Hu, M., and Yan, N. (2014) Crystal structure of the human glucose transporter GLUT1. *Nature* **510**, 121-125
40. Kapoor, K., Finer-Moore, J. S., Pedersen, B. P., Caboni, L., Waight, A., Hillig, R. C., Bringmann, P., Heisler, I., Müller, T., Siebeneicher, H., and Stroud, R. M. (2016) Mechanism of inhibition of human glucose transporter GLUT1 is conserved between cytochalasin B and phenylalanine amides. *Proceedings of the National Academy of Sciences* **113**, 4711-4716
41. Carruthers, A., DeZutter, J., Ganguly, A., and Devaskar, S. U. (2009) Will the original glucose transporter isoform please stand up! *American Journal of Physiology-Endocrinology and Metabolism* **297**, E836-E848
42. Lowe, A. G., and Walmsley, A. R. (1986) The kinetics of glucose transport in human red blood cells. *Biochimica et Biophysica Acta (BBA) - Biomembranes* **857**, 146-154

43. Fischbarg, J., Kuang, K. Y., Hirsch, J., Lecuona, S., Rogozinski, L., Silverstein, S. C., and Loike, J. (1989) Evidence that the glucose transporter serves as a water channel in J774 macrophages. *Proceedings of the National Academy of Sciences* **86**, 8397
44. Ke, M., Yuan, Y., Jiang, X., Yan, N., and Gong, H. (2017) Molecular determinants for the thermodynamic and functional divergence of uniporter GLUT1 and proton symporter XylE. *PLOS Computational Biology* **13**, e1005603
45. Park, M.-S. (2015) Molecular Dynamics Simulations of the Human Glucose Transporter GLUT1. *PLOS ONE* **10**, e0125361
46. Fu, X., Zhang, G., Liu, R., Wei, J., Zhang-Negrerie, D., Jian, X., and Gao, Q. (2016) Mechanistic Study of Human Glucose Transport Mediated by GLUT1. *Journal of Chemical Information and Modeling* **56**, 517-526
47. Galochkina, T., Ng Fuk Chong, M., Challali, L., Abbar, S., and Etchebest, C. (2019) New insights into GluT1 mechanics during glucose transfer. *Scientific Reports* **9**, 998
48. Jardetzky, O. (1966) Simple Allosteric Model for Membrane Pumps. *Nature* **211**, 969
49. Iglesias-Fernandez, J., Quinn, P. J., Naftalin, R. J., and Domene, C. (2017) Membrane Phase-Dependent Occlusion of Intramolecular GLUT1 Cavities Demonstrated by Simulations. *Biophysical Journal* **112**, 1176-1184
50. Liang, H., Bourdon, A. K., Chen, L. Y., Phelix, C. F., and Perry, G. (2018) Gibbs Free-Energy Gradient along the Path of Glucose Transport through Human Glucose Transporter 3. *ACS Chemical Neuroscience* **11**, 2815-2823
51. Wambo, T. O., Chen, L. Y., Phelix, C., and Perry, G. (2017) Affinity and path of binding xylopyranose unto E. coli xylose permease. *Biochemical and Biophysical Research Communications* **494**, 202-206
52. Hresko, R. C., Kraft, T. E., Quigley, A., Carpenter, E. P., and Hruz, P. W. (2016) Mammalian Glucose Transporter Activity Is Dependent upon Anionic and Conical Phospholipids. *Journal of Biological Chemistry* **291**, 17271-17282
53. Chen, L. Y., and Phelix, C. F. (2019) Extracellular Gating of Glucose Transport through GLUT 1. *Biochemical and Biophysical Research Communications* **511**, 573-578
54. Kahlenberg, A., and Banjo, B. (1972) Involvement of Phospholipids in the d-Glucose Uptake Activity of Isolated Human Erythrocyte Membranes. *Journal of Biological Chemistry* **247**, 1156-1160
55. O'Brien, J. S., and Sampson, E. L. (1965) Lipid composition of the normal human brain: gray matter, white matter, and myelin. *Journal of Lipid Research* **6**, 537-544
56. Spector, A. A., and Yorek, M. A. (1985) Membrane lipid composition and cellular function. *Journal of Lipid Research* **26**, 1015-1035
57. Baaden, M. (2019) Visualizing Biological Membrane Organization and Dynamics. *Journal of Molecular Biology* **431**, 1889-1919
58. Corradi, V., Sejdiu, B. I., Mesa-Galloso, H., Abdizadeh, H., Noskov, S. Y., Marrink, S. J., and Tieleman, D. P. (2019) Emerging Diversity in Lipid–Protein Interactions. *Chemical Reviews* **119**, 5775-5848
59. Jacobson, K., Liu, P., and Lagerholm, B. C. (2019) The Lateral Organization and Mobility of Plasma Membrane Components. *Cell* **177**, 806-819
60. Muller, M. P., Jiang, T., Sun, C., Lihan, M., Pant, S., Mahinthichaichan, P., Trifan, A., and Tajkhorshid, E. (2019) Characterization of Lipid–Protein Interactions and Lipid-Mediated Modulation of Membrane Protein Function through Molecular Simulation. *Chemical Reviews* **119**, 6086-6161
61. Aoun, M., Corsetto, P. A., Nugue, G., Montorfano, G., Ciusani, E., Crouzier, D., Hogarth, P., Gregory, A., Hayflick, S., Zorzi, G., Rizzo, A. M., and Tiranti, V. (2017) Changes in Red Blood Cell

membrane lipid composition: A new perspective into the pathogenesis of PKAN. *Molecular Genetics and Metabolism* **121**, 180-189

62. Virtanen, J. A., Cheng, K. H., and Somerharju, P. (1998) Phospholipid composition of the mammalian red cell membrane can be rationalized by a superlattice model. *Proceedings of the National Academy of Sciences* **95**, 4964
63. Chen, L. Y. (2013) Glycerol modulates water permeation through Escherichia coli aquaglyceroporin GlpF. *Biochimica et Biophysica Acta (BBA) - Biomembranes* **1828**, 1786-1793
64. Best, R. B., Zhu, X., Shim, J., Lopes, P. E. M., Mittal, J., Feig, M., and MacKerell, A. D. (2012) Optimization of the Additive CHARMM All-Atom Protein Force Field Targeting Improved Sampling of the Backbone φ, ψ and Side-Chain χ1 and χ2 Dihedral Angles. *Journal of Chemical Theory and Computation* **8**, 3257-3273
65. Vanommeslaeghe, K., and MacKerell Jr, A. D. (2015) CHARMM additive and polarizable force fields for biophysics and computer-aided drug design. *Biochimica et Biophysica Acta (BBA) - General Subjects* **1850**, 861-871
66. Phillips, J. C., Braun, R., Wang, W., Gumbart, J., Tajkhorshid, E., Villa, E., Chipot, C., Skeel, R. D., Kalé, L., and Schulten, K. (2005) Scalable molecular dynamics with NAMD. *J. Comput. Chem.* **26**, 1781-1802
67. Jo, S., Kim, T., Iyer, V. G., and Im, W. (2008) CHARMM-GUI: A web-based graphical user interface for CHARMM. *Journal of Computational Chemistry* **29**, 1859-1865
68. Lee, J., Cheng, X., Swails, J. M., Yeom, M. S., Eastman, P. K., Lemkul, J. A., Wei, S., Buckner, J., Jeong, J. C., Qi, Y., Jo, S., Pande, V. S., Case, D. A., Brooks, C. L., MacKerell, A. D., Klauda, J. B., and Im, W. (2016) CHARMM-GUI Input Generator for NAMD, GROMACS, AMBER, OpenMM, and CHARMM/OpenMM Simulations Using the CHARMM36 Additive Force Field. *Journal of Chemical Theory and Computation* **12**, 405-413

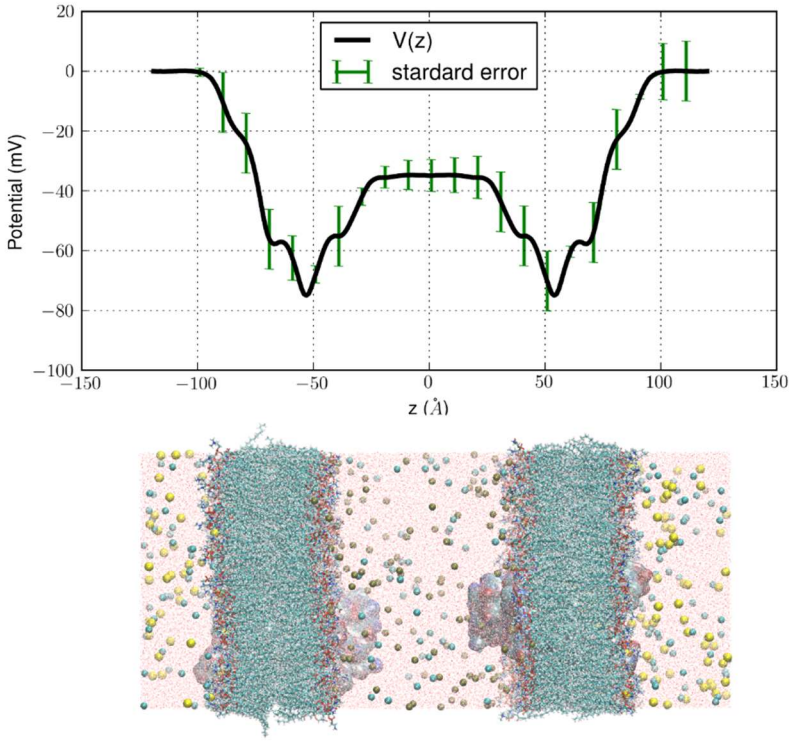

Figure 1. Electrostatic potential computed from the charge distribution sampled from the last 100 ns of the 500 ns MD run. The bottom panel illustrates the model system. The two membrane patches (shown in licorices) are located at $-90\text{Å} < z < -40\text{Å}$ and at $40\text{Å} < z < 90\text{Å}$. The two proteins (proteins 0 on the left and 1 on the right) are shown in surfaces. The water molecules are shown in dots and ions in spheres. All colored by elements/atoms (H, white; C, cyan; O, red; N, blue, P, red; S, yellow; Cl, cyan; Na, yellow; K, metallic).

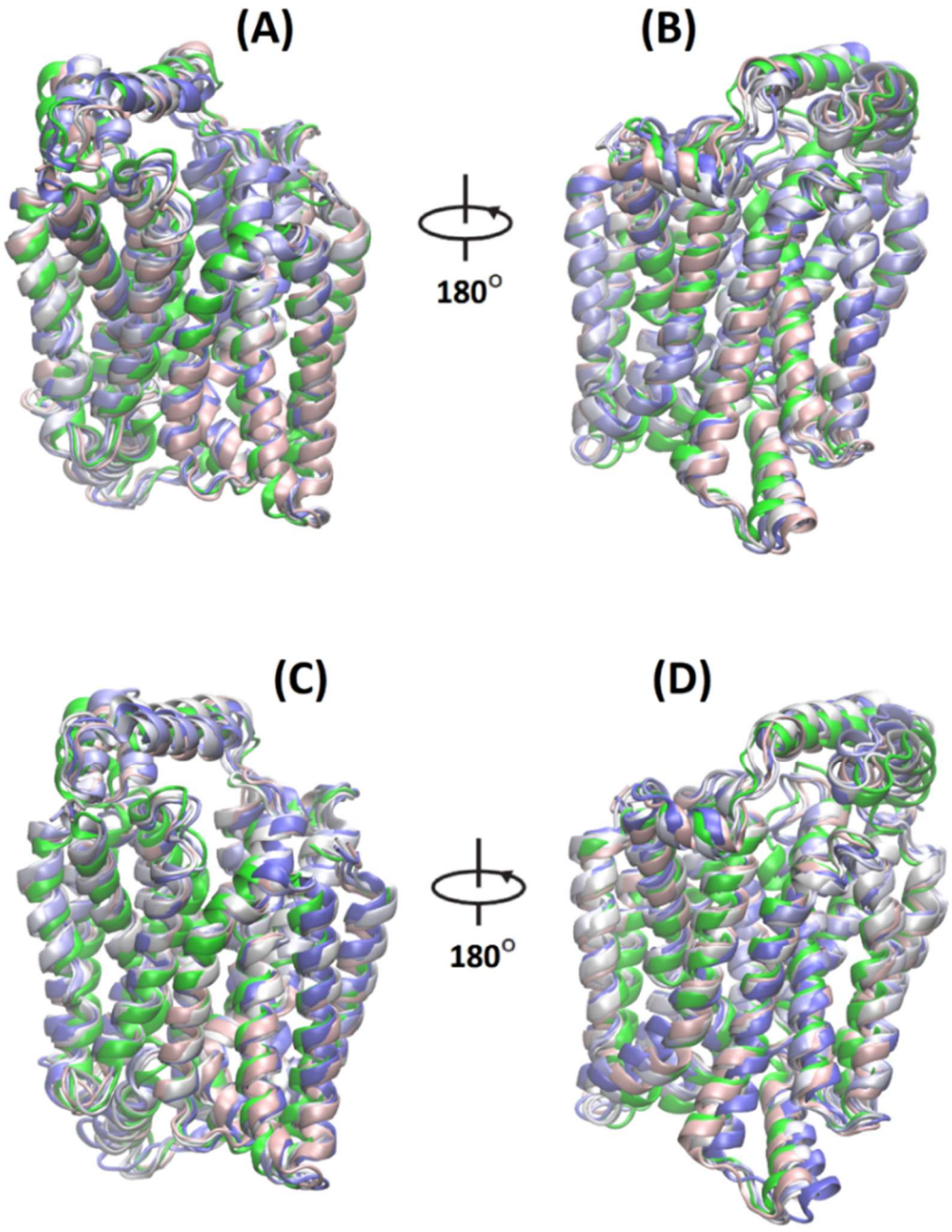

Figure 2. Deviations of GLUT1 from the crystal structure during 500 ns MD run. (A) and (B) show the snapshot structures (grayish blues) of protein 0 at 100, 200, … and 500 ns overlapped on the crystal structure (green). (C) and (D), *i.b.i.d.* for protein 1.

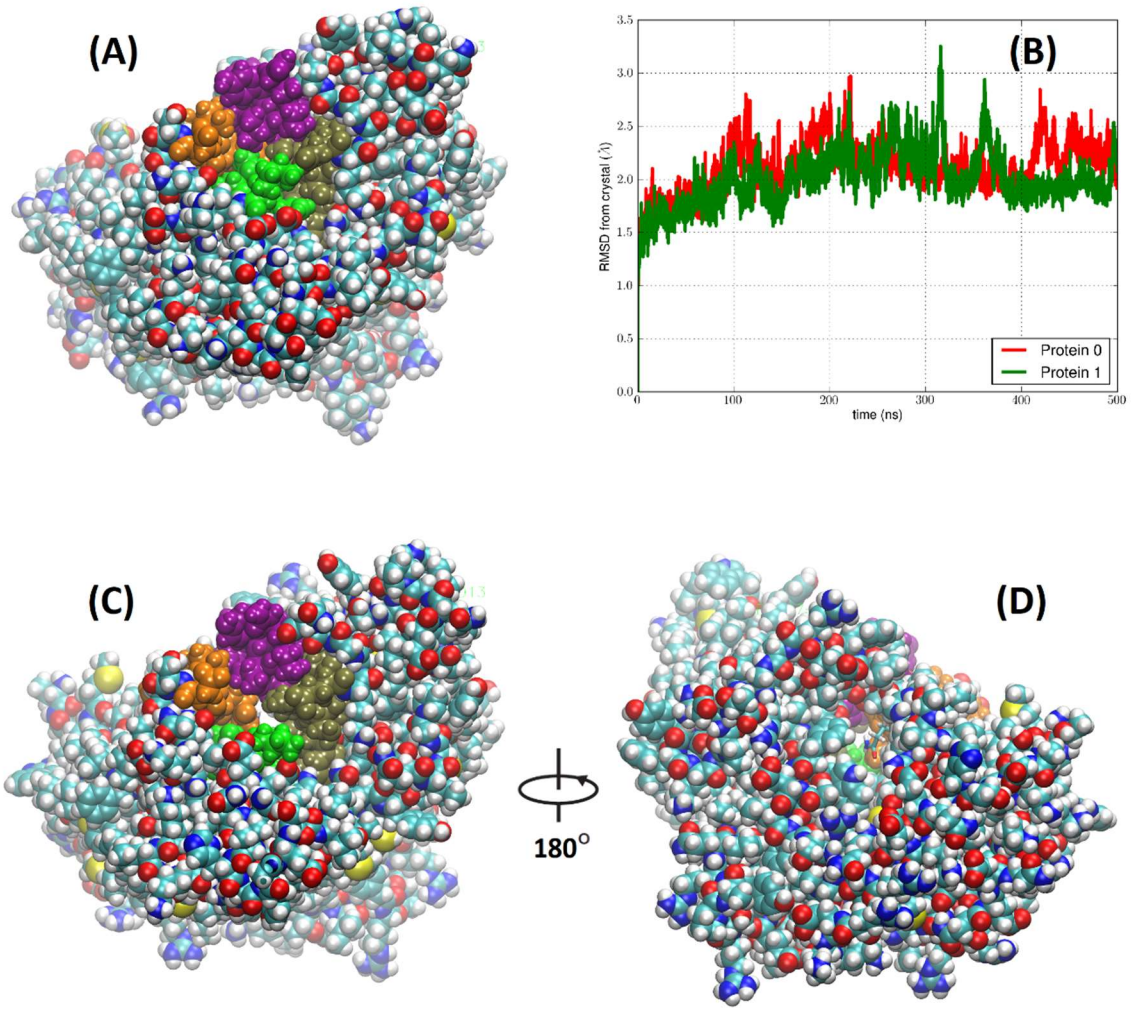

Figure 3. Crystal structure *vs.* dynamic snapshot structure of GLUT1 showing EC-gate closed/open. (A), (C) and (D) show the protein in space-filling spheres. (B) shows the RMSD from the crystal structure during 500 ns of MD run. The EC-gate residues are colored by the TMs they are on while all other residues colored by atoms (H, white; O, red; C, cyan; N, blue; S, yellow). (A) EC view of the protein crystal structure showing the EC gate closed. (C) EC view of the open EC gate. (D) IC view of the open EC gate. Gln 161 is shown in licorices because, if shown in space-filling spheres, it would obscure the view of the EC-gate even though it does not block the access to the binding site and the EC gate from the IC side.

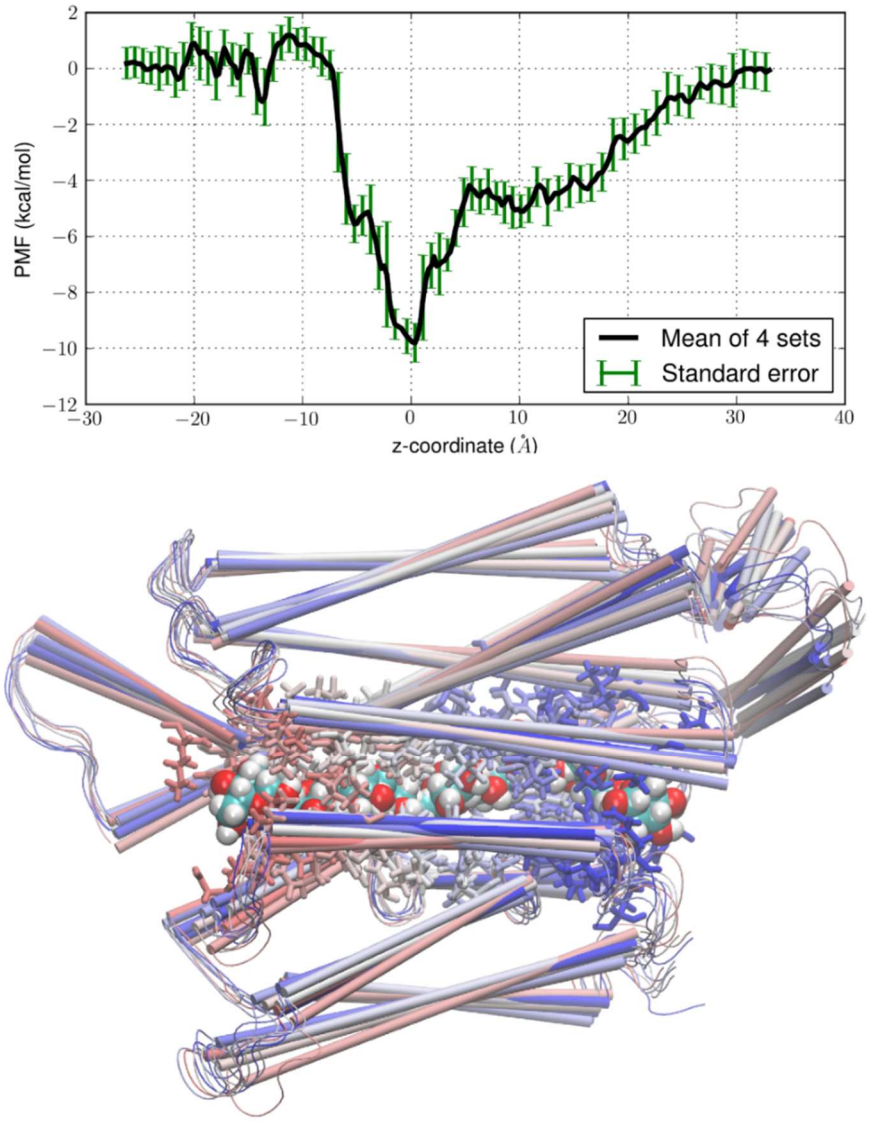

Figure 4. Glucose transport path of diffusion facilitated by GLUT1. Top, PMF of glucose along the diffusion path computed from SMD simulations. The PMF(z) represents the Gibbs free energy of the system when the center-of-mass z-coordinate of glucose is at a given position. Bottom, glucose (space-filling spheres), GLUT1 (thin cartoons), and residues within 5 Å of glucose (licorices) shown in representative frames along the transport path. The sugar is colored in red (O), cyan (C), and white (H) in all frames but the protein is colored by the fame.